Compressive characteristics and low frequency damping of aluminium matrix syntactic foams

Bálint KATONA[a], Attila SZLANCSIK[a,b], Tamás TÁBI[c,d], Imre Norbert ORBULOV[a,b,*]

[a]MTA–BME Lendület Composite Metal Foams Research Group, Műegyetem rakpart 3., Budapest, Hungary, 1111

[b]Department of Materials Science and Engineering, Faculty of Mechanical Engineering, Budapest University of Technology and Economics, Műegyetem rakpart 3., Budapest, Hungary, 1111

[c]Department of Polymer Engineering, Faculty of Mechanical Engineering, Budapest University of Technology and Economics, Műegyetem rakpart 3., Budapest, Hungary, 1111

[d]MTA–BME Research Group for Composite Science and Technology, Műegyetem rakpart 3., Budapest, Hungary, 1111

*Corresponding author

Address: Department of Materials Science and Engineering, Faculty of Mechanical Engineering, Budapest University of Technology and Economics, Műegyetem rakpart 3., Budapest, Hungary, 1111

Tel: +36 1 463 2386

Fax: +36 1 463 1366

E-mail: orbulov@eik.bme.hu

Abstract

Al99.5 and AlSi12 matrix syntactic foams were produced by pressure infiltration of Globocer grade ceramic hollow spheres. The produced aluminium matrix syntactic foams (AMSFs) were investigated by compressive tests, dynamic mechanical analysis (DMA), finite element methods (DMA) and elasticity based analytical calculations. The aim of the investigations was (i) to map the compressive properties of the AMSFs, (ii) to determine and compare the effective Young's modulus of the AMSFs determined by compressive tests, DMA, FEM and analytical calculations and (iii) to determine the low frequency damping capability of the AMSFs. The compressive tests showed pronounced differences between the two matrix materials, characterized by higher compressive strength, compressive strain and absorbed mechanical energy in the case of AlSi12 matrix, however, the energy absorption efficiency due to the different failure mechanism of AMSFs (homogeneous densification in the case of Al99.5 and cleavage in the case of AlSi12 matrix, respectively). The DMA tests confirmed the effective Young's moduli values, measured by compression and proved higher damping capability in the case of AlSi12 matrix. FEM and analytical calculations also confirmed the measured effective Young's moduli within a reasonable error band.

Keywords: aluminium matrix syntactic foam, composite metal foam, effective Young's modulus, dynamic mechanical analysis, damping.

1 Introduction

Aluminium matrix syntactic foams (AMSFs) are a special class of the metallic foams. They can be defined as structural materials with pores, in which the porosity is ensured by incorporating hollow spheres into the metallic matrix. The hollow spheres are more or less ordered to each other and they are dispersed homogenously. Between the metallic matrix and the hollow spheres an interface layer can be formed. Such foams are also often called composite metal foams (CMFs) in the literature [1,2]. The interface layer can be cohesive (if there is a chemical reaction between the constituents) or adhesive. The interface layer is reliable for the proper load transfer between the matrix and the hollow spheres. One of the most attractive features of AMSFs is in the possibility to vary their mechanical properties within wide ranges by planned selection of the matrix material and by the correct selection of the material and size of the hollow spheres. The volume fraction of the hollow spheres also has significant effect on the properties of the AMSFs. Moreover – like other metallic foams – AMSFs have good specific mechanical properties, which are isotropic contrary to liquid state produced 'conventional' metallic foams (because the lack of gravitational force effects, that has no role on the geometry of pores in the case of AMSFs). The matrix material of AMSFs is some kind of aluminium alloy usually; however, similar structures (in general metal matrix syntactic foams (MMSFs)) with steel [1,3–5], magnesium [6–13], titanium [14–17] and zinc [18–22] matrices have also been reported. The filler or reinforcing hollow spheres can be ceramic or metallic in material and they are commercially available from specified providers, such as Hollomet GmbH [23], for example. Additional serious efforts have been made to reduce the cost of AMSFs by using low cost perlite [24–33] or pumice [34]. As the main load mode of metallic foams is compression, the compressive properties of AMSFs have been widely studied in different conditions (for example in quasi-static or in dynamic conditions in the aspect of load rates) [35–69]. Due to its importance, the compressive test methodology and characteristic properties under quasi-static conditions have been summarized in standard procedures [70,71]. Besides the strength and deformation values, the

standard describes the ‘elastic gradient’ and ‘quasi-elastic gradient’ of the material, that can be identified rather as a structural stiffness (depending on the actual spatial structure of the foam) than an effective Young’s modulus (that is the Young’s modulus of a fictive homogeneous isotropic body substituting the AMSFs).

The above-mentioned publications are dealing with the compression of AMSFs with a primary focus on the strength properties and load bearing capability. However, the effective elastic modulus and damping capability are important in the aspect of design and operation too, since AMSFs can be applied as extremely light, high stiffness structural parts or as collision or vibration dampers. Dynamic mechanical analysis (DMA) is a test in which an oscillating (in our case sinusoidal) force is applied on a three-point bending sample and the corresponding deformation is determined as a reply. The main outcomes of the test are the complex modulus (representing the effective elastic modulus of the material), the storage modulus (representing the elastic portion), the loss modulus (representing the dissipation) and the damping of the investigated samples. The temperature and / or the load frequency can be varied during the test, therefore the materials properties can be investigated in a wider range. DMA is also capable to provide information of phase transformations in the material; however, in the aspect of the AMSFs, the mechanical properties are more important. In the field of metallic foams DMA tests are extensively applied to map the mechanical properties and damping with respect to the temperature and load frequency [8,45,64]. In summary, the main findings in the aspect of mechanical properties of the above cited DMA tests are: (i) the storage modulus of a foam is always smaller than the base materials’; (ii) the loss modulus and the damping parameter of a foam is always higher compared to the base materials’ properties and (iii) the temperature dependence of the moduli are varying according to the investigated material. The DMA test was applied because it can provide precise data on the effective elastic modulus of the material due to its sophisticated measurement method, with respect to the temperature.

Regarding the effective Young’s modulus, the main problem is in the early plastic deformation of the material due to even small compressive load as it is detailed in [49] and in [72]. Therefore, the determination of the effective Young’s modulus is not a trivial problem, the main difficulty is in the correct and precise measurement of the extremely small deformation. It can be measured by extremely sensitive and low load compression tests, however the friction phenomena in the loading frame and tools as well as the extremely small deformations is challenging. Another, but indirect possibility is to model the compressive test in finite element environment in which small loads and deformations can be easily modelled. Finally, the effective Young’s modulus can be calculated. In this field Bardella [73–77] and Marur [78–81] published the most relevant articles highlighting the possibilities and limits of these elasticity based theoretical homogenization models. Two of them, namely the differential self-consistent (DSC) and the Mori-Tanaka (MT) methods were proved to give correct estimation on the effective Young’s modulus in the case of AMSFs [82].

Besides the overall compressive characterization of the studied AMSFs (characteristic properties, failure mechanisms), the first aim of this paper is to compare the moduli resulted from the different methods (physical compression tests (i), their finite element model (ii), DMA (iii) and analytical calculations (iv)) at room and at elevated temperatures. Secondly, the determination of the low frequency damping properties of AMSFs is aimed also in the function of temperature, as a direct result from the DMA measurements.

2 Materials and methods

Al99.5 and AlSi12 aluminium alloys were applied as matrix materials, their chemical compositions are listed in Table 1. (measured by energy dispersive spectrometry (EDS)). The hollow spheres (Globocer grade) were provided by Hollomet GmbH [23]. The chemical composition of the hollow spheres was measured to be 33 wt% Al_2O_3, 48 wt% SiO_2 and 19 wt% $3Al_2O_3{\cdot}2SiO_2$ (mullite). The average diameter and wall thickness of the spheres were Ø1425 ± 42.2 µm and 60 ± 1.7 µm, respectively, while their density was 0.816 gcm^{-3}. The AMSFs were produced by pressure infiltration technique with ~45 vol% hollow sphere content. The infiltration pressure and time was set to 400 kPa and 30 s, respectively, while the infiltration temperature was set to 50°C above the melting temperature of matrix (660 + 50°C for the Al99.5 and 575 + 50°C for the AlSi12 alloy, respectively). The applied infiltration method is described in details in previous publications [83–85]. The produced AMSF blocks were sectioned and cylindrical samples (Ø15 × 22.5 mm) for classic compression tests, while rectangular bar samples for DMA tests (7 × 10 × 50 mm) were machined.

Table 1. Chemical composition of matrices (in wt%, measured by EDS)

Matrix	Si	Fe	Cu	Mn	Mg	Zn	Al
Al99.5	0.250	0.400	0.050	0.050	0.050	0.050	rem.
AlSi12	12.830	0.127	0.002	0.005	0.003	0.007	rem.

The conventional compression tests were performed on an Instron 5965 universal materials testing machine equipped with a 5 kN load cell and a 0.0001 mm precision extensometer. The samples were placed between grinded and polished plates (65 HRC) without guiding bars in order to minimize the effect of friction on the measurement. Both sides of the samples were carefully lubricated with Locktite anti-seize lube. Six specimens were compressed for each matrix material.

The DMA tests were performed on a DMA Q800 type DMA tester in three-point bending mode with a span length of 35 mm. The temperature ramp was set to 10°C/min and the tests were conducted from 0°C up to 380°C. The applied frequency was 1 Hz, while the amplitude was 5 µm. The tests were repeated on two samples from each matrix grade.

The FEM investigations were performed in Marc Mentat® environment .Four point tetrahedral elements were applied to mesh the geometry with average side length of 350 µm. The whole modell was built up from 350 000 elements. The interface layers in the AMSFs between the hollow spheres and the actual matrix material assumed to be perfect, therefore the nodes of the outer surface of the hollow spheres and the matrix material were merged. The matrix materials in the model were considered elastic-plastic, while the ceramic hollow spheres assumed to be completely elastic. The compression tests were run up to 1000 N compressive load. The model was compressed between rigid plates assuming perfect lubrication between the cylindrical sample and the plates (µ=0).The analytical calculations were performed by the DSC and the MT methods, based on [73–77]. Both model predicts the bulk (K) and the shear (G) modulus of the materials from which the effective Young's modulus can be calculated based on the basic relationships of elasticity. These methods are described briefly in Section 3.4.

3 Results and Discussion

3.1 Compression tests

The average curves (black) and their corresponding standard deviation bands (grey) along with the lower (blue) and upper (red) boundary curves are plotted in Fig. 1. in engineering stress – engineering strain system.

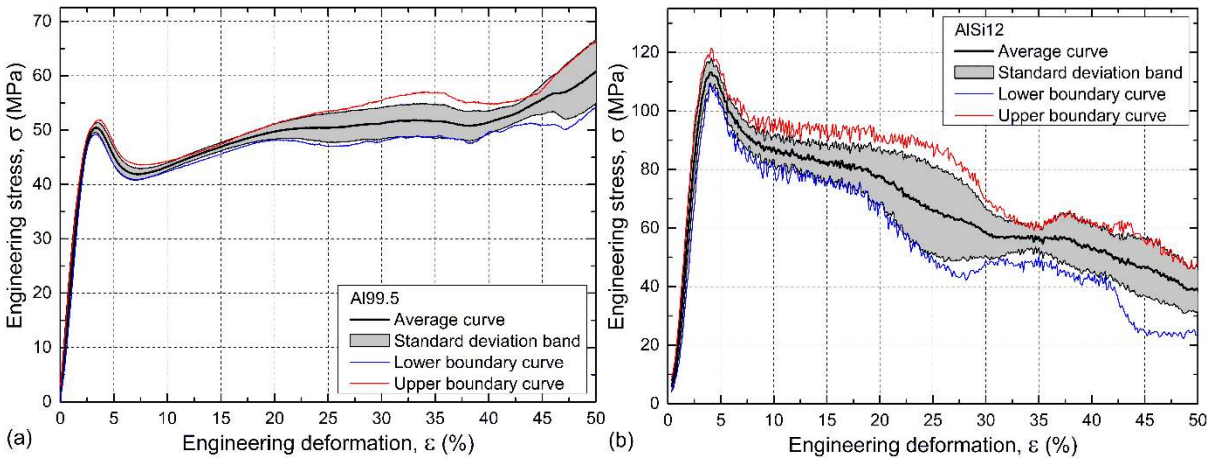

Fig. 1. The average compressive curves of (a) Al99.5 and (b) AlSi12 matrix AMSFs

Qualitatively, the recorded curves show a few similarity and difference. Both of the curves can be divided into three parts as in most cases regarding metallic foams. The first part exhibits linear relationship between the engineering stress and engineering strain, that ends in a local peak that corresponds to the compressive strength. The compressive peak is followed by a stress drop due to the appearance of the first crack in the sample (relaxation). Subsequently, a plateau region developed according to the actual failure mechanism of the sample. The plateau region can show (i) ascending or (ii) descending trends as it is detailed below corresponding to the matrix material. Starting with the Al99.5 matrix AMSF (Fig. 2.), the compressive flow strength of the matrix was initially lower than the crush strength of the hollow spheres. Therefore, the deformation was homogeneous in the whole sample during the first few percent of the deformation, the hollow spheres moved like rigid bodies and the first failed hollow spheres appeared in the middle of the sample (most complex stress state) at the compressive strength. This deformation mechanism was observed in [41,49] and was explained by the plasticity and strength of the matrix material. The curvature in the vicinity of the compressive strength was low, plotting a quite blunt peak that indicates an equalized and slow deformation mechanism. The subsequent plastic deformation resulted in a moderately increasing plateau region and continuous failure of the neighbouring hollow spheres (see the lower part of Fig. 2b). The process ended in almost perfect densification (Fig. 2c). Further analysing the recorded curve, the standard deviation band along the plateau region remained narrow, proving well repeatable amount of absorbed mechanical energy. The whole engineering stress – engineering strain curve is smooth and free from sudden changes and / or drops.

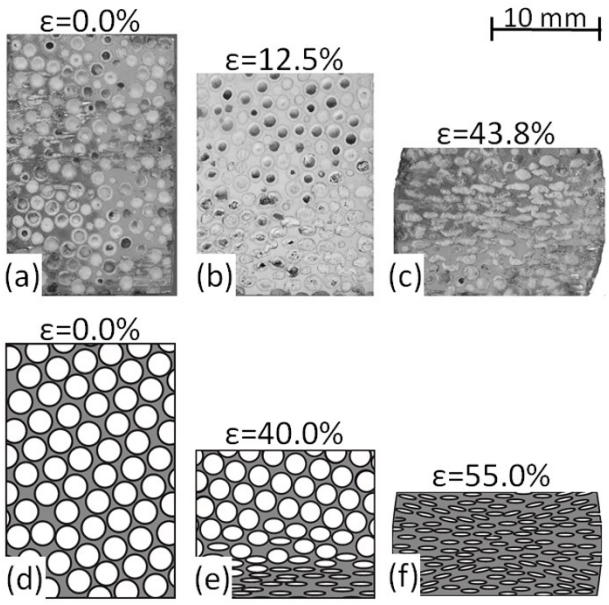

Fig. 2. Deformation mechanism of Al99.5 matrix AMSFs: (a-c) example and (d-f) schematic process

In the case of AlSi12 matrix, the initial flow strength of the alloyed matrix exceeded the crush strength of the hollow spheres resulting in a more sudden stress drop curve (higher curvature in the vicinity of the compressive strength) after the stress peak at the end of the linear section of the compressive. This stress drop can be connected to the appearance of a pronounced crack along a ~45° line (maximal shear stress) to the load direction (dashed lines in fig. 3a). Along the crack line (Figs. 3b, 3c, 3e and 3f) the hollow spheres were broken and sheared in the direction of the crack surface. The initial crack divided the sample into two halves and the failure mechanism proceeded along this initial crack surface by the slow sliding of the sample halves. This phenomenon resulted in (i) an extensively ragged engineering stress – engineering deformation curve after the compressive strength peak, (ii) a continuously declining plateau region, since the material was not deforming anymore (the halves were only sliding on each other) and (iii) a relatively wide standard deviation band. Other parts of the material remained unharmed (Figs. 3d and 3h). In some cases, close to the crack line, a part of the hollow spheres could be also broken (Fig. 3g), however these hollow spheres were crushed in the direction of the load (similar to the Al99.5 matrix AMSFs), due to the additional forces awaken when the sliding sample part started to contact the counterpart of the compressive tool.

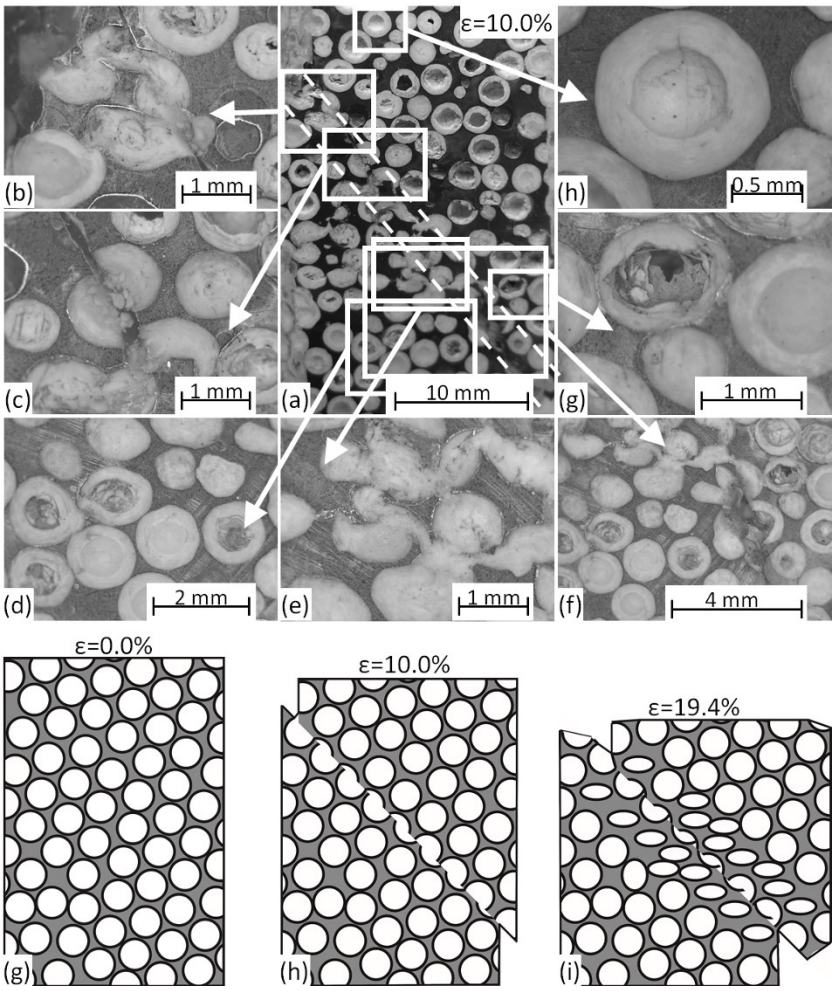

Fig. 3. Deformation mechanism of AlSi12 matrix AMSFs (a-h) and the schematic process (i-k)

Quantitatively, the compressive tests were evaluated according to the ruling standard [71] (except the effective Young's modulus) and hereby the characteristic properties are reported in Table 2. The effective Young's modulus was measured by fitting a line on the low load part (<10 MPa) of the measured compressive curves to minimize the possible plastic deformations, that are measured in the stiffness if the standard methods apply (see 'elastic gradient' and 'quasi-elastic gradient' in [71]).

Table 2. Characteristic compressive properties of the investigated foams

Property	Designation	Unit	Al99.5	AlSi12
First maximum compressive strength	σ_C	MPa	50.3 ± 0.6	114.4 ± 5.2
Deformation at compressive strength	ε_C	%	3.33 ± 0.17	4.25 ± 0.32
Effective Young's modulus	E	GPa	21.9 ± 1.2	22.2 ± 2.4
Plateau strength	$\sigma_{Pl,20-40}$	MPa	51.0 ± 2.2	57.2 ± 1.4
Energy absorption at 50% deformation	W_{50}	MJm^{-3}	24.5 ± 0.8	32.2 ± 0.6
Energy absorption efficiency	η_W	%	97.3 ± 2.2	56.4 ± 1.8

The studied AMSFs showed quite different behaviour according to the basic properties of the matrices. The alloyed and higher strength AlSi12 alloy (UTS 115 MPa against the 75 MPa UTS of

Al99.5) resulted in more than twice as large compressive strength (σ_C) as in the case of the Al99.5 alloy. On the other hand, one may expect lower deformation at the compressive strength (ε_C) due to the rigidity of the near eutectic AlSi12 alloy. However, a moderate increment can be observed because of the presence of the hollow spheres that sheared under the increasing load balancing the rigidity of the Si alloyed matrix by introducing some kind of virtual plasticity. As it can be seen in the case of the effective Young's modulus, the 10 GPa difference in the Young's modulus of the matrices (Tables 2 and 4 below) decreased to ~1 GPa, in other words, the effective Young's modulus of the AMSFs were mainly influenced by the presence of the hollow spheres.

3.2 DMA tests

The temperature dependent DMA curves (storage modulus, loss modulus and loss factor) are shown in Fig. 4. The storage modulus (E') is the proportionality factor between the elastic deformation and the applied stress. The loss modulus (E") corresponds to the energy dissipated in one loading cycle due to the internal frictions and deformations in the material, while the damping parameter (tanδ) is the ratio of the loss and the storage moduli and in connection to the ratio of the dissipated and stored energy in the material during one load cycle. Moreover, this damping parameter determines a phase lag between the response of the strain due to the applied load and corresponds to the damping characteristics of the material, however only at the loading frequency, that is usually low (1 Hz in this case). From the above-mentioned moduli, the complex modulus (often referred as 'dynamic' modulus in the literature) can be calculated according to eq. 1.

$$E = \sqrt{E'^2 + E''^2} \tag{1}$$

In the case of a DMA test this complex modulus corresponds to the effective Young's modulus, that is able to describe the overall behaviour of the material at low loads.

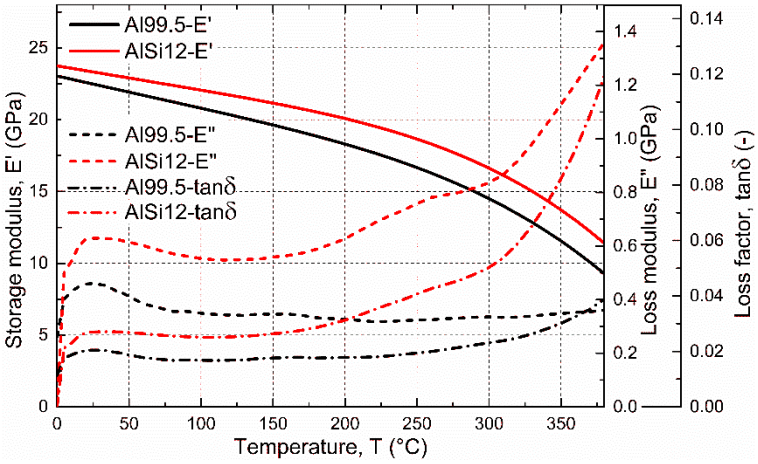

Fig. 4. DMA curves of the investigated MMSFs

In the function of temperature, the storage moduli decreased together in the case of both matrices. The AlSi12 composition showed a slightly better performance (lower decrement) at higher temperatures, due to the relatively high Si content, that can be observed in the form of blocky primary Si particles (arrows in Fig. 5) near to the Globocer hollow spheres and Si needles (Fig. 5b).

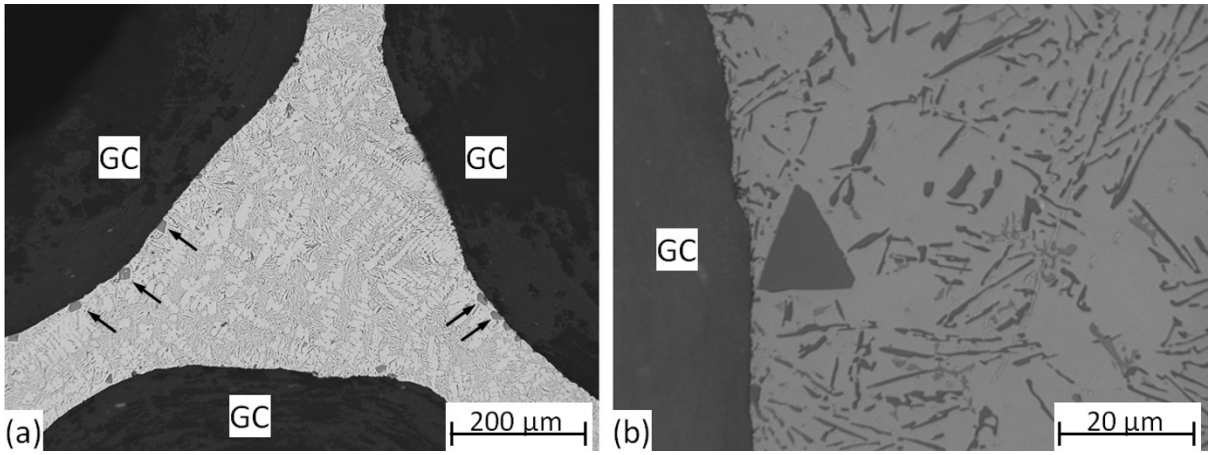

Fig. 5. Micrographs of an AlSi12 matrix sample

In Fig. 5a three hollow spheres can be seen (designated by 'GC' labels). Between them the microstructure of the matrix shows eutectic structure with Al dendrites. Close to the spheres small and bulky Si particles are situated (a few of them are highlighted by arrows). For better visualization, the vicinity of a particle is shown in Fig. 5b in higher magnification, in which both the bulk Si particles and the Si lamellae in the eutectic structure can be clearly observed. The loss modulus of the AMSFs were proved to be one magnitude lower compared to the storage modulus indicating a moderate damping capability as can be observed on the rightmost scale in Fig. 4. Above ~200°C the loss modulus of the AlSi12 based AMSFs started to increase, while the Al99.5 based AMSFs maintained the ~0.38 GPa loss modulus level. The increasing loss modulus can be connected to the presence of the Si precipitation in the matrix, resulting in higher internal friction, than in the case of Al99.5 alloy [72] (similar phenomenon to the case of lamellar cast irons). In the case of Si alloying in the matrix and at higher temperatures (T>200°C), the monotonically decreasing storage and the increasing loss moduli resulted in a raising damping parameter. Contrary, the damping parameter of Al99.5 based AMSFs remained almost constant and slightly increased only above ~300°C due to the moderate decrement in storage modulus. This means that at higher temperature the Si containing material is capable to accommodate higher amount of dissipated energy, therefore it would be better for vibration damping applications for example. On the other hand, the damping parameter of Al99.5 AMSFs remains constant in a wider temperature range, therefore it is easier to design for such materials in low frequency damping applications. The effective Young's moduli of the AMSFs are summarized in the 'DMA' column in Table 4, since the loss moduli are two magnitudes lower than the storage moduli, practically the latter can be considered as effective Young's modulus with the values of 22.3 GPa and 22.9 GPa at 20°C or 18.3 GPa and 20.1 GPa at 200°C in the case of Al99.5 and AlSi12 based AMSFs, respectively (Table 4).

3.3 Finite element analysis

The compression tests were modelled in virtual environment by FEM. In order to provide the most similar conditions, a full, 3D model was created. As a first step in model creation, the hollow spheres were distributed randomly in the given volume identical in size to the real compression samples (Ø15 × 22.5 mm) with the produced ~45 vol% volume fraction. The output of the algorithm is a list describing the positions, diameters and wall-thickness of the distributed hollow spheres. These data were implemented in the FEM software to generate the 3D model firstly by subtracting the volume

of the hollow spheres and secondly by adding the walls of the ceramic hollow spheres. The whole 3D model was meshed by four node tetrahedral elements, allowing large deformations (Fig. 6a). As a result, the force – displacement values were registered, and the data were transformed into engineering stress versus engineering strain plot from which the effective Young's modulus, represented by the slope of the curve can be obtained (Fig. 6b). The whole procedure was repeated for 20°C and for 200°C as well and the corresponding effective Young's modulus of 26.5 GPa and 29.5 GPa were determined for Al99.5 and AlSi12, respectively at 20°C, while at 200°C 21.5 GPa and 24.2 GPa were calculated for Al99.5 and AlSi12 matrices, respectively (Table 4).

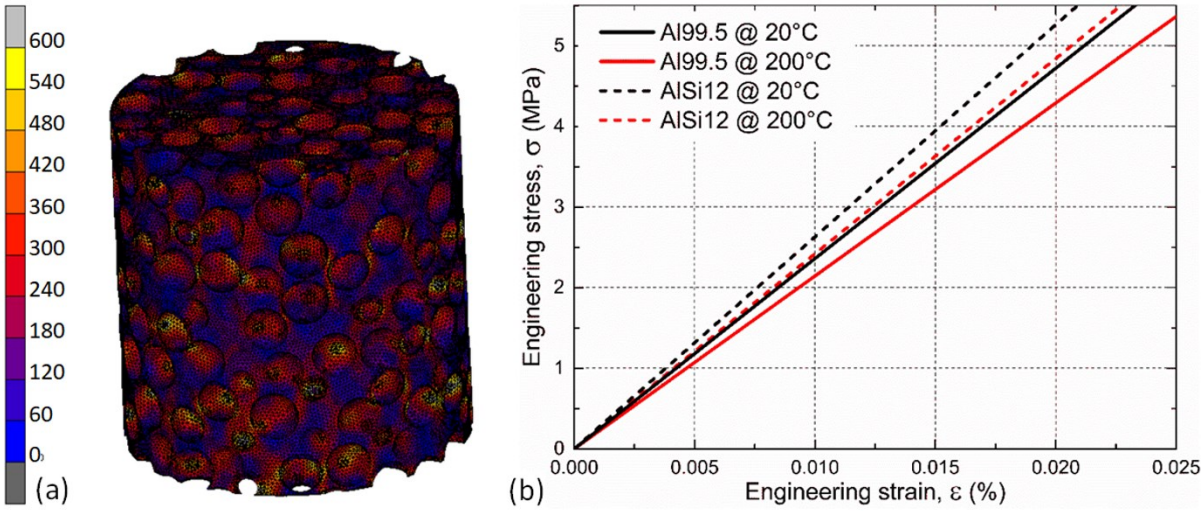

Fig. 6. FEM model of AMSFs highlighting the von Mises stress distribution (a) and stress versus strain plots of the FEM results (b)

3.4 Analytical models

Hereby, the equations of the DSC and MT models were applied to calculate the elastic properties, especially the effective Young's modulus [73–77]. The differential equations of the DSC estimations are detailed in eqs. 2 and 3:

$$\frac{dK_{DSC}(f)}{df} = \frac{1}{1-f}\left(\frac{(1-\eta^3)K_{DSC}(f)(K_s-K_{DSC}(f))}{K_{DSC}(f)+\alpha(f)(K_s-K_{DSC}(f))} + \frac{\eta^3 K_{DSC}(f)}{\alpha(f)-1}\right) \quad (2)$$

$$\frac{dG_{DSC}(f)}{df} = \frac{1}{1-f}\left(\frac{(1-\eta^3)G_{DSC}(f)(G_s-G_{DSC}(f))}{K_{DSC}(f)+\beta(f)(G_s-G_{DSC}(f))} + \frac{\eta^3 G_{DSC}(f)}{\beta(f)-1}\right) \quad (3)$$

where 'f' is the filler's volume fraction, 'η' is the radius ratio (the ratio of the inner and outer radius of the hollow spheres), subscript 's' denotes the property of the hollow spheres and finally α and β are determined by (eqs. 4 and 5):

$$\alpha = \frac{3K}{3K+4G} \quad (4)$$

$$\beta = \frac{6(K+2G)}{5(3K+4G)} \quad (5)$$

The initial value of the DSC estimation are the bulk matrix properties, where the filler volume fraction (f) is 0. The explicit Euler method was used to solve the differential equations. The

definitions of the bulk (K, eq. 6) and shear (G, eq. 7) moduli by the Mori-Tanaka estimation are the followings:

$$K_{MT} = \frac{(1-f)K_m + f(1-\eta^3)\frac{3K_S K_m}{(3K_S+4G_m)\alpha_m}}{f\eta^3\frac{3K_m}{4G_m} - f(1-\eta^3)\frac{3(K_S-K_m)}{3K_S+4G_m}+1} \quad (6)$$

$$G_{MT} = \frac{(1-f)G_m + f(1-\eta^3)\frac{G_m}{\left(1+\frac{G_m(9K_m+8G_m)}{6G_S(K_m+2G_m)}\right)\beta_m}}{f\eta^3\frac{6(K_m-2G_m)}{9K_m+8G_m} - f(1-\eta^3)\frac{G_S-G_m}{G_S+\frac{G_m(9K_m+8G_m)}{6(K_m+2G_m)}}+1} \quad (7)$$

where subscript m stands for the properties of the matrix material. The properties applied for the calculations are listed in Table 3. For both matrices the Poisson ratio was assumed to be ν=0.33. The properties of the hollow spheres' wall were calculated by simple rule of mixture, according to the chemical composition of the hollow spheres (see Section 2.). As the properties of constituents, for the alumina $E_{alumina}$=400 GPa and $\nu_{alumina}$=0.24, for the mullite $E_{mullite}$=130 GPa and $\nu_{mullite}$=0.24 and for the silica E_{silica}=70 GPa and ν_{silica}=0.17 were used in the calculations, respectively. The calculations resulted in hollow spheres' properties of $E_{hollow\ spheres}$=190 GPa and $\nu_{hollow\ spheres}$=0.21. The shear modulus and the bulk modulus were derived from the Young's modulus and Poisson ratio according to the elasticity equations (Eqs. 8 and 9).

$$G = \frac{E}{2(1+\upsilon)} \quad (8)$$

$$K = \frac{E}{3(1-2\upsilon)} \quad (9)$$

Table 3. Materials properties used for the calculations at 20°C and at 200°C

Property	Designation	Unit	Al99.5		AlSi12		Globocer	
			RT	200°C	RT	200°C	RT	200°C
Young's modulus	E	GPa	70.1	63.6	79.1	71.8	190.0	185.4
Shear modulus	G	GPa	26.3	23.9	29.3	27.0	78.5	76.6
Bulk modulus	K	GPa	68.6	62.4	76.5	70.4	109.2	106.6

Corresponding to the DSC model, the calculations resulted in an effective Young's modulus of 20.9 GPa at 20°C and 17.6 GPa at 200°C in the case of Al99.5 and 23.4 GPa at 20°C and 19.9 GPa at 200°C in the case of AlSi12 matrix, while the MT model gave 26.5 GPa at 20°C and 22.9 GPa at 200°C in the case of Al99.5 and 29.6 GPa at 20°C and 25.9 GPa at 200°C in the case of AlSi12 matrix, respectively. In summary and for better clarity, the determined effective Young's moduli are listed in Table 4.

Table 4. Effective Young's moduli of matrix materials and AMSFs at 20°C and at 200°C

E (GPa)	Compression	DMA		FEM		Analytical DSC method		Analytical MT method	
	20°C	20°C	200°C	20°C	200°C	20°C	200°C	20°C	200°C
Al99.5 MMSF	21.9 ± 1.2	22.3	18.3	23.6	21.5	20.9	17.6	26.5	22.9
AlSi12 MMSF	22.2 ± 2.4	22.9	20.1	26.3	24.2	23.4	19.9	29.6	25.9

Regarding the 20°C results, listed in Table 4 the FEM model and the MT calculations slightly overestimated the measured (compression test and DMA) moduli values. The physically measured values showed almost perfect agreement in the case of both matrix materials. Comparing the analytical results, the DSC method ensured better estimation. Considering the elevated test temperature (200°C) results the same trends can be concluded: the FEM and the MT methods gave a slight overestimation, while the DSC method resulted in a more punctual estimation of the effective Young's modulus.

4 Conclusions

From the investigations and discussion detailed above, the following conclusions can be drawn. Regarding the compressive tests of Al99.5 and AlSi12 alloy based, Globocer ceramic hollow sphere filled AMSFs:

- The AlSi12 based AMSFs proved higher compressive strength, higher deformation at compressive strength and higher absorbed mechanical energy.
- Contrary to the absorbed energy (in absolute value and up to 50% deformation), the energy absorption efficiency was higher in the case of Al99.5 matrix material. The reason is in the different failure mechanisms: (i) homogeneous densification in the case of Al99.5 and (ii) cleavage in the case of AlSi12 matrix, respectively.
- Considering the effective Young's modulus, the values for Al99.5 and AlSi12 based AMSFs were very similar, therefore this property is mainly influenced by the incorporated hollow spheres and less by the matrix material.

Regarding the DMA tests:

- The loss moduli were two magnitudes lower compared to the storage moduli, resulting in moderate low frequency damping capability.
- The loss modulus and the damping parameter were higher in the case of AlSi12 matrix due to the presence of blocky and lamellar Si precipitations (similar to lamellar cast irons). The difference was more pronounced at higher temperatures, especially above 200°C.
- The damping parameter increased or remained constant with the temperature in the case of AlSi12 or Al99.5 matrices, respectively.

Comparing the results of compression and DMA tests, a good correlation can be found in the effective Young's moduli, the average difference was below 2.5% on the basis of the results from compression tests.

Regarding the FEM simulations, the model ensured an acceptable approximation for the effective Young's moduli, however slightly overestimated the measured values both at 20°C and at elevated temperature (200°C).

Regarding the elasticity based analytical calculations, the DSC and MT methods both confirmed the measured effective Young's moduli of AMSFs, however the DSC method proved to be a more precise estimation. Similarly to the FEM results, the MT method slightly overestimated the measured effective Young's moduli.

Acknowledgement

The research reported in this paper was supported by the Higher Education Excellence Program of the Ministry of Human Capacities in the frame of Nanotechnology research area of Budapest University of Technology and Economics (BME FIKP-NANO).

Data availability

The raw/processed data required to reproduce these findings cannot be shared at this time as the data also forms part of an ongoing study

References

[1] A. Rabiei, M. Garcia-Avila, Effect of various parameters on properties of composite steel foams under variety of loading rates, Mater. Sci. Eng. A. 564 (2013) 539–547. doi:10.1016/j.msea.2012.11.108.

[2] Y. Alvandi-Tabrizi, D.A. Whisler, H. Kim, A. Rabiei, High strain rate behavior of composite metal foams, Mater. Sci. Eng. A. 631 (2015) 248–257. doi:10.1016/j.msea.2015.02.027.

[3] G. Castro, S.R. Nutt, Synthesis of syntactic steel foam using gravity-fed infiltration, Mater. Sci. Eng. A. 553 (2012) 89–95. doi:10.1016/j.msea.2012.05.097.

[4] G. Castro, S.R. Nutt, Synthesis of syntactic steel foam using mechanical pressure infiltration, Mater. Sci. Eng. A. 535 (2012) 274–280. doi:10.1016/j.msea.2011.12.084.

[5] L. Peroni, M. Scapin, C. Fichera, D. Lehmhus, J. Weise, J. Baumeister, M. Avalle, Investigation of the mechanical behaviour of AISI 316L stainless steel syntactic foams at different strain-rates, Compos. Part B Eng. 66 (2014) 430–442. doi:10.1016/j.compositesb.2014.06.001.

[6] G. Anbuchezhiyan, B. Mohan, D. Sathianarayanan, T. Muthuramalingam, Synthesis and characterization of hollow glass microspheres reinforced magnesium alloy matrix syntactic foam, J. Alloys Compd. (2017). doi:10.1016/j.jallcom.2017.05.153.

[7] K.N. Braszczyńska-Malik, J. Kamieniak, Analysis of interface between components in AZ91 magnesium alloy foam composite with Ni-P coated fly ash cenospheres, J. Alloys Compd. 720 (2017) 352–359. doi:10.1016/j.jallcom.2017.05.285.

[8] H. Anantharaman, V.C. Shunmugasamy, O.M. Strbik, N. Gupta, K. Cho, Dynamic properties of silicon carbide hollow particle filled magnesium alloy (AZ91D) matrix syntactic foams, Int. J. Impact Eng. 82 (2015) 14–24. doi:10.1016/j.ijimpeng.2015.04.008.

[9] X. Xia, J. Wang, Y. Peng, N. Wang, X. He, C. Qiu, J. Ding, X. Chen, Temperature-Time Superposition Effect on Compressive Properties of AZ31B Magnesium Composite Foams, Met. . 8 (2018). doi:10.3390/met8060434.

[10] K.N. Braszczyńska-Malik, J. Kamieniak, The Role of Ni-P Coating Structure on Fly Ash Cenospheres in the Formation of Magnesium Matrix Composites, Metall. Mater. Trans. A. (2017). doi:10.1007/s11661-017-4272-x.

[11] X. Xia, J. Feng, J. Ding, K. Song, X. Chen, W. Zhao, B. Liao, B. Hur, Fabrication and characterization of closed-cell magnesium-based composite foams, Mater. Des. 74 (2015) 36–43. doi:10.1016/j.matdes.2015.02.029.

[12] K.N. Braszczyńska-Malik, J. Kamieniak, AZ91 magnesium matrix foam composites with fly ash cenospheres fabricated by negative pressure infiltration technique, Mater. Charact. 128

(2017) 209–216. doi:10.1016/j.matchar.2017.04.005.

[13] A. Daoud, M.T. Abou El-khair, M. Abdel-Aziz, P. Rohatgi, Fabrication, microstructure and compressive behavior of ZC63 Mg–microballoon foam composites, Compos. Sci. Technol. 67 (2007) 1842–1853. doi:10.1016/j.compscitech.2006.10.023.

[14] N. Jha, D.P. Mondal, M.D. Goel, J.D. Majumdar, S. Das, O.P. Modi, Titanium cenosphere syntactic foam with coarser cenosphere fabricated by powder metallurgy at lower compaction load, Trans. Nonferrous Met. Soc. China. 24 (2014) 89–99. doi:10.1016/S1003-6326(14)63032-6.

[15] S. Kashef, A. Asgari, T.B. Hilditch, W. Yan, V.K. Goel, P.D. Hodgson, Fracture toughness of titanium foams for medical applications, Mater. Sci. Eng. A. 527 (2010) 7689–7693. doi:10.1016/j.msea.2010.08.044.

[16] S. Kashef, A. Asgari, T.B. Hilditch, W. Yan, V.K. Goel, P.D. Hodgson, Fatigue crack growth behavior of titanium foams for medical applications, Mater. Sci. Eng. A. 528 (2011) 1602–1607. doi:10.1016/j.msea.2010.11.024.

[17] D.P. Mondal, J. Datta Majumder, N. Jha, A. Badkul, S. Das, A. Patel, G. Gupta, Titanium-cenosphere syntactic foam made through powder metallurgy route, Mater. Des. 34 (2012) 82–89. doi:10.1016/j.matdes.2011.07.055.

[18] L. Pan, Y. Yang, M.U. Ahsan, D.D. Luong, N. Gupta, A. Kumar, P.K. Rohatgi, Zn-Matrix Syntactic Foams: Effect of Heat Treatment on Microstructure and Compressive Properties, Mater. Sci. Eng. A. (2018). doi:10.1016/j.msea.2018.06.072.

[19] Manoj, D.M. Afzal Khan, D.P. Mondal, High temperature deformation behavior of closed cell ZnAl27 hybrid foam made through stir casting technique, Mater. Sci. Eng. A. 731 (2018) 324–330. doi:10.1016/j.msea.2018.06.044.

[20] J.A. Aragon-Lezama, A. Garcia-Borquez, G. Torres-Villaseñor, Foam behavior of solid glass spheres – Zn22Al2Cu composites under compression stresses, Mater. Sci. Eng. A. 638 (2015) 165–173. doi:10.1016/j.msea.2015.04.048.

[21] A. Daoud, Effect of strain rate on compressive properties of novel Zn12Al based composite foams containing hybrid pores, Mater. Sci. Eng. A. 525 (2009) 7–17. doi:10.1016/j.msea.2009.05.038.

[22] A. Sánchez-Martínez, A. Cruz, M. González-Nava, M.A. Suárez, Main process parameters for manufacturing open-cell Zn-22Al-2Cu foams by the centrifugal infiltration route and mechanical properties, Mater. Des. 108 (2016) 494–500. doi:10.1016/j.matdes.2016.07.032.

[23] Hollomet GmbH, (n.d.). http://www.hollomet.com/en/home.html (accessed May 4, 2018).

[24] M. Borovinšek, M. Taherishargh, M. Vesenjak, Z. Ren, T. Fiedler, Geometrical characterization of perlite-metal syntactic foam, Mater. Charact. 119 (2016) 209–215. doi:10.1016/j.matchar.2016.07.024.

[25] S. Broxtermann, M. Taherishargh, I.V. Belova, G.E. Murch, T. Fiedler, On the compressive behaviour of high porosity expanded Perlite-Metal Syntactic Foam (P-MSF), J. Alloys Compd. 691 (2017) 690–697. doi:10.1016/j.jallcom.2016.08.284.

[26] M. Taherishargh, I.V. Belova, G.E. Murch, T. Fiedler, The effect of particle shape on mechanical properties of perlite/metal syntactic foam, J. Alloys Compd. 693 (2017) 55–60. doi:10.1016/j.jallcom.2016.09.168.

[27] M. Taherishargh, B. Katona, T. Fiedler, I.N. Orbulov, Fatigue properties of expanded

perlite/aluminum syntactic foams, J. Compos. Mater. 51 (2017) 773–781. doi:10.1177/0021998316654305.

[28] T. Fiedler, I.V. Belova, G.E. Murch, On the thermal properties of expanded perlite – Metallic syntactic foam, Int. J. Heat Mass Transf. 90 (2015) 1009–1014. doi:10.1016/j.ijheatmasstransfer.2015.07.049.

[29] M.A. Sulong, M. Taherishargh, I.V. Belova, G.E. Murch, T. Fiedler, On the mechanical anisotropy of the compressive properties of aluminium perlite syntactic foam, Comput. Mater. Sci. 109 (2015) 258–265. doi:10.1016/j.commatsci.2015.07.038.

[30] M. Taherishargh, I.V. Belova, G.E. Murch, T. Fiedler, Low-density expanded perlite–aluminium syntactic foam, Mater. Sci. Eng. A. 604 (2014) 127–134. doi:10.1016/j.msea.2014.03.003.

[31] M. Taherishargh, M.A. Sulong, I.V. Belova, G.E. Murch, T. Fiedler, On the particle size effect in expanded perlite aluminium syntactic foam, Mater. Des. 66 (2015) 294–303. doi:10.1016/j.matdes.2014.10.073.

[32] M. Taherishargh, I.V. Belova, G.E. Murch, T. Fiedler, On the mechanical properties of heat-treated expanded perlite–aluminium syntactic foam, Mater. Des. 63 (2014) 375–383. doi:10.1016/j.matdes.2014.06.019.

[33] T. Fiedler, M. Taherishargh, L. Krstulović-Opara, M. Vesenjak, Dynamic compressive loading of expanded perlite/aluminum syntactic foam, Mater. Sci. Eng. A. 626 (2015) 296–304. doi:10.1016/j.msea.2014.12.032.

[34] M. Taherishargh, I.V. Belova, G.E. Murch, T. Fiedler, Pumice/aluminium syntactic foam, Mater. Sci. Eng. A. 635 (2015) 102–108. doi:10.1016/j.msea.2015.03.061.

[35] X. Xia, X. Chen, Z. Zhang, X. Chen, W. Zhao, B. Liao, B. Hur, Compressive properties of closed-cell aluminum foams with different contents of ceramic microspheres, Mater. Des. 56 (2014) 353–358. doi:10.1016/j.matdes.2013.11.040.

[36] M.D. Goel, V.A. Matsagar, A.K. Gupta, Blast resistance of stiffened sandwich panels with aluminum cenosphere syntactic foam, Int. J. Impact Eng. 77 (2015) 134–146. doi:10.1016/j.ijimpeng.2014.11.017.

[37] G.H. Wu, Z.Y. Dou, D.L. Sun, L.T. Jiang, B.S. Ding, B.F. He, Compression behaviors of cenosphere–pure aluminum syntactic foams, Scr. Mater. 56 (2007) 221–224. doi:10.1016/j.scriptamat.2006.10.008.

[38] A. Szlancsik, B. Katona, K. Májlinger, I.N. Orbulov, Compressive Behavior and Microstructural Characteristics of Iron Hollow Sphere Filled Aluminum Matrix Syntactic Foams, Materials (Basel). 8 (2015) 7926–7937. doi:10.3390/ma8115432.

[39] Z.Y. Dou, L.T. Jiang, G.H. Wu, Q. Zhang, Z.Y. Xiu, G.Q. Chen, High strain rate compression of cenosphere-pure aluminum syntactic foams, Scr. Mater. 57 (2007) 945–948. doi:10.1016/j.scriptamat.2007.07.024.

[40] D.D. Luong, N. Gupta, A. Daoud, P.K. Rohatgi, High strain rate compressive characterization of aluminum alloy/fly ash cenosphere composites, JOM. 63 (2011) 53–56. doi:10.1007/s11837-011-0029-y.

[41] D.K. Balch, D.C. Dunand, Load partitioning in aluminum syntactic foams containing ceramic microspheres, Acta Mater. 54 (2006) 1501–1511. doi:10.1016/j.actamat.2005.11.017.

[42] I.N. Orbulov, A. Szlancsik, On the Mechanical Properties of Aluminum Matrix Syntactic Foams, Adv. Eng. Mater. (2018). doi:10.1002/adem.201700980.

[43] M.D. Goel, D.P. Mondal, M.S. Yadav, S.K. Gupta, Effect of strain rate and relative density on compressive deformation behavior of aluminum cenosphere syntactic foam, Mater. Sci. Eng. A. 590 (2014) 406–415. doi:10.1016/j.msea.2013.10.048.

[44] D.D. Luong, O.M. Strbik, V.H. Hammond, N. Gupta, K. Cho, Development of high performance lightweight aluminum alloy/SiC hollow sphere syntactic foams and compressive characterization at quasi-static and high strain rates, J. Alloys Compd. 550 (2013) 412–422. doi:10.1016/j.jallcom.2012.10.171.

[45] L. Licitra, D.D. Luong, O.M. Strbik, N. Gupta, Dynamic properties of alumina hollow particle filled aluminum alloy A356 matrix syntactic foams, Mater. Des. 66 (2015) 504–515. doi:10.1016/j.matdes.2014.03.041.

[46] L.J. Vendra, A. Rabiei, A study on aluminum–steel composite metal foam processed by casting, Mater. Sci. Eng. A. 465 (2007) 59–67. doi:10.1016/j.msea.2007.04.037.

[47] D.P. Mondal, N. Jha, A. Badkul, S. Das, R. Khedle, High temperature compressive deformation behaviour of aluminum syntactic foam, Mater. Sci. Eng. A. 534 (2012) 521–529. doi:10.1016/j.msea.2011.12.002.

[48] L.C. Zou, Q. Zhang, B.J. Pang, G.H. Wu, L.T. Jiang, H. Su, Dynamic compressive behavior of aluminum matrix syntactic foam and its multilayer structure, 2013. doi:10.1016/j.matdes.2012.08.015.

[49] D.K. Balch, J.G. O'Dwyer, G.R. Davis, C.M. Cady, G.T. Gray, D.C. Dunand, Plasticity and damage in aluminum syntactic foams deformed under dynamic and quasi-static conditions, Mater. Sci. Eng. A. 391 (2005) 408–417. doi:10.1016/j.msea.2004.09.012.

[50] C.A. Vogiatzis, A. Tsouknidas, D.T. Kountouras, S. Skolianos, Aluminum–ceramic cenospheres syntactic foams produced by powder metallurgy route, Mater. Des. 85 (2015) 444–454. doi:10.1016/j.matdes.2015.06.154.

[51] K. Myers, B. Katona, P. Cortes, I.N. Orbulov, Quasi-static and high strain rate response of aluminum matrix syntactic foams under compression, Compos. Part A Appl. Sci. Manuf. 79 (2015) 82–91. doi:10.1016/j.compositesa.2015.09.018.

[52] M.D. Goel, M. Peroni, G. Solomos, D.P. Mondal, V.A. Matsagar, A.K. Gupta, M. Larcher, S. Marburg, Dynamic compression behavior of cenosphere aluminum alloy syntactic foam, 2012. doi:10.1016/j.matdes.2012.06.013.

[53] S. Birla, D.P. Mondal, S. Das, A. Khare, J.P. Singh, Effect of cenosphere particle size and relative density on the compressive deformation behavior of aluminum-cenosphere hybrid foam, Mater. Des. 117 (2017) 168–177. doi:10.1016/j.matdes.2016.12.078.

[54] M.Y. Omar, C. Xiang, N. Gupta, O.M. Strbik, K. Cho, Data characterizing flexural properties of Al/Al2O3 syntactic foam core metal matrix sandwich, Data Br. 5 (2015) 564–571. doi:10.1016/j.dib.2015.09.054.

[55] L.P. Zhang, Y.Y. Zhao, Mechanical Response of Al Matrix Syntactic Foams Produced by Pressure Infiltration Casting, J. Compos. Mater. 41 (2007) 2105–2117. doi:10.1177/0021998307074132.

[56] J.A. Santa Maria, B.F. Schultz, J.B. Ferguson, N. Gupta, P.K. Rohatgi, Effect of hollow sphere size and size distribution on the quasi-static and high strain rate compressive properties of Al-A380--Al2O3 syntactic foams, J. Mater. Sci. 49 (2014) 1267–1278. doi:10.1007/s10853-013-7810-y.

[57] J.A. Santa Maria, B.F. Schultz, J.B. Ferguson, P.K. Rohatgi, Al–Al2O3 syntactic foams – Part I: Effect of matrix strength and hollow sphere size on the quasi-static properties of Al-A206/Al2O3 syntactic foams, Mater. Sci. Eng. A. 582 (2013) 415–422. doi:10.1016/j.msea.2013.05.081.

[58] D.P. Mondal, S. Das, N. Ramakrishnan, K. Uday Bhasker, Cenosphere filled aluminum syntactic foam made through stir-casting technique, Compos. Part A Appl. Sci. Manuf. 40 (2009) 279–288. doi:10.1016/j.compositesa.2008.12.006.

[59] Y. Lin, Q. Zhang, X. Ma, G. Wu, Mechanical behavior of pure Al and Al–Mg syntactic foam composites containing glass cenospheres, Compos. Part A Appl. Sci. Manuf. 87 (2016) 194–202. doi:10.1016/j.compositesa.2016.05.001.

[60] I.N. Orbulov, Compressive properties of aluminium matrix syntactic foams, Mater. Sci. Eng. A. 555 (2012) 52–56. doi:10.1016/j.msea.2012.06.032.

[61] M. DASS GOEL, V.A. MATSAGAR, A.K. GUPTA, S. MARBURG, Strain rate sensitivity of closed cell aluminium fly ash foam, Trans. Nonferrous Met. Soc. China. 23 (2013) 1080–1089. doi:10.1016/S1003-6326(13)62569-8.

[62] A. Szlancsik, B. Katona, K. Bobor, K. Májlinger, I.N. Orbulov, Compressive behaviour of aluminium matrix syntactic foams reinforced by iron hollow spheres, Mater. Des. 83 (2015) 230–237. doi:10.1016/j.matdes.2015.06.011.

[63] I.N. Orbulov, K. Májlinger, Characterisation of hybrid metal matrix syntactic foams, 2015. doi:10.4028/www.scientific.net/MSF.812.219.

[64] J. Cox, D.D. Luong, V.C. Shunmugasamy, N. Gupta, O.M. Strbik, K. Cho, Dynamic and Thermal Properties of Aluminum Alloy A356/Silicon Carbide Hollow Particle Syntactic Foams, Metals (Basel). 4 (2014) 530–548. doi:10.3390/met4040530.

[65] G. Castro, S.R. Nutt, X. Wenchen, Compression and low-velocity impact behavior of aluminum syntactic foam, Mater. Sci. Eng. A. 578 (2013) 222–229. doi:10.1016/j.msea.2013.04.081.

[66] D.P. Mondal, M.D. Goel, S. Das, Compressive deformation and energy absorption characteristics of closed cell aluminum-fly ash particle composite foam, Mater. Sci. Eng. A. 507 (2009) 102–109. doi:10.1016/j.msea.2009.01.019.

[67] M. Kiser, M.Y. He, F.W. Zok, The mechanical response of ceramic microballoon reinforced aluminum matrix composites under compressive loading, Acta Mater. 47 (1999) 2685–2694. doi:10.1016/S1359-6454(99)00129-9.

[68] A. Szlancsik, B. Katona, K. Májlinger, I.N. Orbulov, Compressive behavior and microstructural characteristics of iron hollow sphere filled aluminum matrix syntactic foams, Materials (Basel). 8 (2015). doi:10.3390/ma8115432.

[69] B. Zhang, Y. Lin, S. Li, D. Zhai, G. Wu, Quasi-static and high strain rates compressive behavior of aluminum matrix syntactic foams, Compos. Part B Eng. 98 (2016) 288–296. doi:10.1016/j.compositesb.2016.05.034.

[70] DIN50134:2008 - Prüfung von meatllischen Werkstoffen - Druckversuch an metallischen zellularen Werkstoffen, (2008).

[71] ISO13314:2011 Mechanical testing of metals - Ductility testing - Compression test for porous and cellular metals, (2011).

[72] C. Kádár, K. Máthis, I.N. Orbulov, F. Chmelík, Monitoring the failure mechanisms in metal matrix syntactic foams during compression by acoustic emission, 2016.

doi:10.1016/j.matlet.2016.02.102.

[73] L. Bardella, F. Genna, On the elastic behavior of syntactic foams, Int. J. Solids Struct. 38 (2001) 7235–7260. doi:10.1016/S0020-7683(00)00228-6.

[74] L. Bardella, An extension of the Secant Method for the homogenization of the nonlinear behavior of composite materials, Int. J. Eng. Sci. 41 (2003) 741–768. doi:10.1016/S0020-7225(02)00276-8.

[75] L. Bardella, F. Genna, Elastic design of syntactic foamed sandwiches obtained by filling of three-dimensional sandwich-fabric panels, Int. J. Solids Struct. 38 (2001) 307–333. doi:10.1016/S0020-7683(00)00025-1.

[76] L. Bardella, A. Sfreddo, C. Ventura, M. Porfiri, N. Gupta, A critical evaluation of micromechanical models for syntactic foams, Mech. Mater. 50 (2012) 53–69. doi:10.1016/j.mechmat.2012.02.008.

[77] A. Panteghini, L. Bardella, On the compressive strength of glass microballoons-based syntactic foams, Mech. Mater. 82 (2015) 63–77. doi:10.1016/j.mechmat.2014.12.005.

[78] P.R. Marur, Estimation of effective elastic properties and interface stress concentrations in particulate composites by unit cell methods, Acta Mater. 52 (2004) 1263–1270. doi:10.1016/j.actamat.2003.11.010.

[79] P.R. Marur, Numerical estimation of effective elastic moduli of syntactic foams, Finite Elem. Anal. Des. 46 (2010) 1001–1007. doi:10.1016/j.finel.2010.07.006.

[80] P.R. Marur, Influence of imperfect interface on the elastic moduli of syntactic foams, Comput. Mater. Sci. 46 (2009) 327–332. doi:10.1016/j.commatsci.2009.03.010.

[81] P.R. Marur, Effective elastic moduli of syntactic foams, 2005. doi:10.1016/j.matlet.2005.02.034.

[82] A. Szlancsik, B. Katona, Z. Dombóvári, I.N. Orbulov, On the effective Young's modulus of metal matrix syntactic foams, Mater. Sci. Technol. 0 (2017) 1–8. doi:10.1080/02670836.2017.1374497.

[83] I. Norbert Orbulov, J. Dobránszky, Producing metal matrix syntactic foams by pressure infiltration, Period. Polytech. Mech. Eng. 52 (2008) 35–42. doi:10.3311/pp.me.2008-1.06.

[84] I.N. Orbulov, J. Ginsztler, Compressive characteristics of metal matrix syntactic foams, Compos. Part A Appl. Sci. Manuf. 43 (2012) 553–561. doi:10.1016/j.compositesa.2012.01.008.

[85] K. Májlinger, I.N. Orbulov, Characteristic compressive properties of hybrid metal matrix syntactic foams, 606 (2014) 248–256. doi:10.1016/j.msea.2014.03.100.